

# Rupturing $C_{60}$ Molecules into Graphene-Oxide-like Quantum Dots: Structure, Photoluminescence, and Catalytic Application

Guanxiong Chen, Zhiwen Zhuo, Kun Ni, Na Yeon Kim, Yuan Zhao, Zongwei Chen, Bin Xiang, Lihua Yang, Qun Zhang, Zonghoon Lee, Xiaojun Wu, Rodney S. Ruoff, and Yanwu Zhu\*

*The large-scale synthesis of graphene-oxide-like quantum dots (GOLQDs) is reported by oxidizing  $C_{60}$  molecules using a modified Hummers method with a yield of  $\approx 25$  wt% readily achieved. The GOLQDs are highly soluble in water and in addition to hexagons have other carbon rings in the structure. They have an average height of  $\approx 1.2$  nm and a diameter distribution of 0.6–2.2 nm after drying on substrates. First-principle calculations indicate that a possible rupturing route may include the insertion of oxygen atoms to C–C bonds in the  $C_{60}$  molecule, followed by rupture of that C–C bonds. The GOLQD suspension has a strong photoluminescence (PL) with peak position dependent on excitation wavelength. The PL is related to the size and emissive traps caused by oxygen-containing groups. The GOLQDs also catalyze the oxidation of benzyl alcohol with a high selectivity.*

## 1. Introduction

Graphene has unique properties and is attracting considerable attention in various research fields.<sup>[1,2]</sup> Pure graphene has a zero band gap,<sup>[3–5]</sup> which may limit its potential applications

in electronic or optoelectronic devices. Thus efforts have been made to opening a band gap, e.g., by utilizing quantum confinement effects<sup>[6]</sup> or edge states.<sup>[7]</sup> Both quantum confinement and edge effects involve the size, shape, and fraction of  $sp^2$  domains in the graphene.<sup>[8–10]</sup> Two typical examples

Dr. G. Chen, Z. Zhuo, K. Ni, Dr. Y. Zhao, Prof. B. Xiang, Prof. L. Yang, Prof. X. Wu, Prof. Y. Zhu  
Key Laboratory of Materials for Energy Conversion  
Chinese Academy of Sciences  
Department of Materials Science and Engineering  
University of Science and Technology of China  
Hefei, Anhui 230026, P. R. China  
E-mail: zhuyanwu@ustc.edu.cn

N. Y. Kim  
School of Materials Science and Engineering  
Ulsan National Institute of Science and Technology (UNIST)  
Ulsan 689-798, South Korea

Z. Chen, Prof. Q. Zhang  
Department of Chemical Physics  
Hefei National Laboratory for Physical Sciences at the Microscale  
University of Science and Technology of China  
Hefei, Anhui 230026, P. R. China

DOI: 10.1002/sml.201501611

Prof. Z. Lee  
Center for Multidimensional Carbon Materials and  
School of Materials Science and Engineering  
Ulsan National Institute of Science and Technology  
Ulsan 689-798, South Korea

Prof. R. S. Ruoff  
Center for Multidimensional Carbon Materials and  
Department of Chemistry and School of Materials Science  
Ulsan National Institute of Science and Technology  
Ulsan 689-798, South Korea



of opening a band gap include the fabrication of graphene nanoribbons (GNRs) and graphene quantum dots (GQDs). Because of the band gap, field effect transistor (FET) devices based on GNRs are able to provide an on-off ratio of up to  $10^7$  at room temperature.<sup>[11–13]</sup> The presence of a band gap in GQDs also makes electron transition possible when electrons are excited by photons. The recombination of excited electrons and holes in GQDs generate photons, leading to photoluminescence (PL).<sup>[14,15]</sup> Thus, GQDs have been considered as candidates for use in optoelectronic devices, bio-imaging, and sensors.<sup>[16,17]</sup>

The synthesis of GQDs has been based on two strategies: bottom-up and top-down. In the bottom-up route, GQDs were fabricated by transforming and/or assembling precursor molecules, such as assembling 3-iodo-4-bromoaniline by stepwise solution chemistry,<sup>[18,19]</sup> converting glucose by microwave-assisted hydrothermal processing<sup>[20]</sup> or carbonizing citric acid by pyrolysis.<sup>[21]</sup> In the top-down approach GQDs were fabricated by cleaving various carbon precursors to quantum dots. In this manner, GQDs have been prepared from graphene oxide by a hydrothermal method<sup>[15]</sup> from graphene<sup>[22]</sup> and carbon nanotubes<sup>[23]</sup> by electrochemical oxidation, from graphite flakes by microwave irradiation,<sup>[24]</sup> and from carbon fibers<sup>[14]</sup> and coal<sup>[25]</sup> by acidic oxidation. The top-down methods generally produce yields of lower than 10 wt%.<sup>[26]</sup> GQDs on a metal substrate were also synthesized by catalytically opening  $C_{60}$  molecules on ruthenium.<sup>[27]</sup> However, the limited amount of GQDs produced and the need for their subsequent transfer may restrict the use of GQDs obtained by this manner. Recently,  $C_{60}$  molecules were opened to form GQDs by a chemical method and a strong PL was observed.<sup>[28]</sup> However, the yield and detailed structure of the GQDs produced are unknown.

Here we report a one-step chemical oxidation method for rupturing  $C_{60}$  molecules into graphene-oxide-like quantum dots (GOLQDs). With a high yield of  $\approx 25$  wt% from a raw  $C_{60}$  precursor, the obtained GOLQDs are highly soluble in water because of the numerous oxygen-containing groups, as is the case for graphene oxide or GQDs produced from it. Density functional theory (DFT) calculations are used to simulate the oxidation process and possible structures of the GOLQDs. When oxygen-containing groups are partially removed by hydrothermal reduction the PL quantum yield is increased, and the excitation lifetime becomes longer. In addition, a remarkable catalytic activity is observed when GOLQDs are used to oxidize benzyl alcohol.

## 2. Results and Discussion

### 2.1. Synthesis and Characterizations

The production of GOLQDs using a modified Hummers method is schematically shown in **Figure 1a**. The Hummers method was initially proposed to oxidize graphite,<sup>[29]</sup> and the preparation of graphite oxide with various modifications of the method has been important in producing graphene materials on a large scale.<sup>[30]</sup> In a typical synthesis, 500 mg of  $C_{60}$  powder was mixed with 25 mL concentrated sulfuric

acid (98% concentration) and stirred in an ice water bath for 10 min. Then, 1.75 g  $KMnO_4$  was slowly added to the mixture and stirred for 24 h at 25 °C. During processing, the color of the mixture changes from black to purple in  $\approx 2$  h, and then to yellow in the next 10 h. After the reaction, the mixture was dialyzed in pure water to obtain the clear final product. A Tyndall effect was observed when a laser beam traversed the dispersion, demonstrating its existence as a colloidal dispersion, as shown in the inset of **Figure 1b**.

Anion impurities measured by ion chromatography (ICS) and cation impurities measured by inductively coupled plasma-atomic emission spectrometry (ICP-AES) in the suspension after dialysis for 6 d include  $SO_4^{2-}$  (12.2 ppm),  $Mn^{4+}$  (18.8 ppm), and  $K^+$  (1.4 ppm). The pH of dialyzed suspension was still 2.25, which may attribute to the ionization of carboxyl groups located at the edges of GOLQDs.<sup>[31]</sup> The zeta potential of the dialyzed suspension (with a concentration of  $0.17 \text{ mg mL}^{-1}$ ) was measured as  $-19.57 \text{ mV}$  at room temperature, and the suspension remained stable without any precipitates observed after storage for 6 months. **Figure 1b** shows an optical image of yellowish powder obtained by freeze-drying the suspension. During freeze-drying process, GOLQDs will assemble to macroaggregates. Scanning electron microscopy (SEM) of the freeze-dried powder (**Figure 1c**) shows that the GOLQDs have aggregated and assembled into nanostructures of sheets, bowls, or fibers. The freeze-dried powder can be readily re-dispersed in pure water with slight stirring, and a stable suspension was obtained with concentrations as high as  $35 \text{ mg mL}^{-1}$ . Thermogravimetric analysis (TGA) of the freeze-dried powder was performed in air, and the result is shown in **Figure S1** (Supporting Information). The weight loss ( $\approx 20.7\%$ ) recorded up to 120 °C could be due to the evaporation of water in the powder. The losses between 120 and 286 °C ( $\approx 35.9\%$ ) and at higher temperatures ( $\approx 33.7\%$ ) are attributed to the removal of oxygen-containing groups and the burning of carbon, respectively.<sup>[32]</sup> Energy dispersive X-ray spectroscopy (EDX; **Figure S1**, Supporting Information) performed on the resulting ash ( $\approx 9.7\%$ ) shows that S, Mn, and K are the main impurities, which are mostly introduced during processing. With eliminating 9.7 wt% of impurities from freeze-dried powder, the production yield of the GOLQD powder is estimated to be about 25 wt% (details in the Supporting Information).

Atomic force microscopy (AFM) was conducted to investigate the surface morphology of GOLQDs cast on a mica substrate (from a suspension with a concentration of  $0.05 \text{ mg mL}^{-1}$ ) followed by drying in air. A typical image is shown in **Figure 2a**. A line profile obtained from the image indicates that the heights of five GOLQDs are 1.61, 0.97, 1.5, 1.13, and 1.03 nm. A statistical distribution obtained from 498 GOLQDs in the AFM image suggests that they have an average thickness of  $\approx 1.2 \text{ nm}$ , which is slightly higher than the typical values (1.0 and 1.1 nm) documented for graphene oxide platelets,<sup>[33,34]</sup> which could be explained by curvature caused by other carbon rings like pentagons, as discussed below. Given that the radius of the AFM tip is comparable to or bigger than the lateral size of the GOLQDs, transmission electron microscopy (TEM) was used to investigate the morphology and structure of GOLQDs cast and dried from

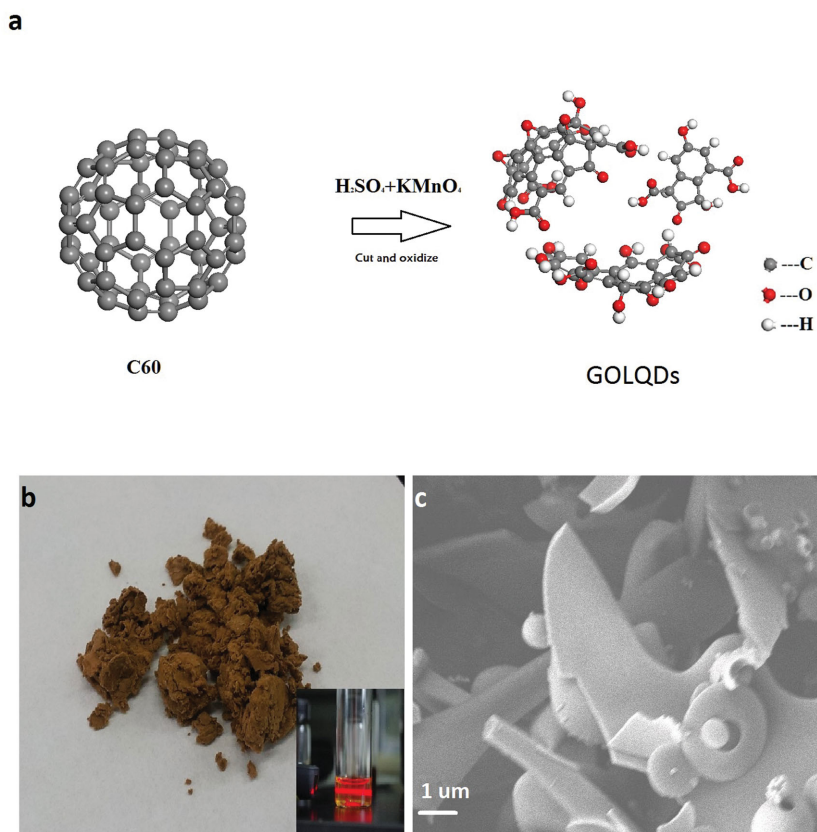


**Figure 1.** a) Schematic of the synthesis of GOLQDs from  $C_{60}$  molecules using a modified Hummers method. b) Optical image of yellowish GOLQD powder obtained by freeze-drying. The inset shows the Tyndall effect of the GOLQD suspension. c) SEM of freeze-dried GOLQDs.

the suspension. From the TEM image shown in Figure 2b and more TEM images shown in Figure S2 (Supporting Information), one can clearly identify GOLQDs lying on the amorphous carbon film on Cu grids. The lateral size measured from 138 GOLQDs in the TEM image shows that GOLQDs have a size distribution between 0.6 and 2.2 nm.

The FTIR spectrum of GOLQD powder is shown in Figure 2d with that of  $C_{60}$  as a reference. From the spectrum, one can see that the GOLQDs contain oxygen-containing groups, such as epoxy (between 1100 and 1400  $\text{cm}^{-1}$ ), carbonyl ( $\approx 1623 \text{ cm}^{-1}$ ), carboxyl ( $\approx 1719 \text{ cm}^{-1}$ ), and hydroxyl ( $\approx 3410 \text{ cm}^{-1}$ ).<sup>[35]</sup> Similar to the case of graphite oxide, these oxygen-containing groups promote the excellent dispersion of GOLQDs in water. The GOLQD powder was also characterized by X-ray photoelectron spectroscopy (XPS), and the C 1s spectrum is shown in Figure 2e. From the spectrum, four main carbon bonding types, i.e., C–C ( $\approx 284.88 \text{ eV}$ ), C–O ( $\approx 287.08 \text{ eV}$ ), C=O ( $\approx 288.48 \text{ eV}$ ), and –COOH ( $\approx 289.06 \text{ eV}$ ) are determined.<sup>[14]</sup> From the carbon 1s spectrum, the fraction of  $sp^2$  carbons is estimated as  $\approx 53.8\%$ , whereas the remaining fraction of carbons is attributed to the bonds formed between carbon and oxygen/hydrogen.<sup>[36]</sup> The C/O atomic ratio obtained from XPS is 1.12, which is consistent with the result of combustion elemental analysis and indicates that the atomic ratio of C:O:H is 1.13:1.01:1. Electron paramagnetic resonance (EPR) measurements were carried out, with 2,2,6,6-tetramethylpiperidine 1-oxyl (TEMPO)

as a reference, to estimate the amount of unpaired electrons in the GOLQD powder. The results are shown in Figure 2f. Based on the calculation, the concentration of spins was determined to be  $1.9 \times 10^{17} \text{ spins g}^{-1}$  for GOLQDs, compared with a value of  $6.2 \times 10^{15} \text{ spins g}^{-1}$  for  $C_{60}$  (corresponding to  $7.4 \times 10^{-6} \text{ spins per } C_{60} \text{ cage on average}$ ). Here, the nonzero number of spins in  $C_{60}$  may originate from defects in the structures or from impurities. The result suggests that opening the cage of  $C_{60}$  has increased the number of unpaired electrons in GOLQDs, which is probably due to the existence of a large number of functional groups or defects.

Raman spectroscopy was used to investigate structural changes after  $C_{60}$  molecules were processed with the modified Hummers method. Typical Raman spectra of as-purchased  $C_{60}$  and as-prepared GOLQD powders are shown in Figure 3a,b. As can be seen, the breathing modes of the  $C_{60}$  cage located at lower wave numbers in the spectrum completely vanished after the  $C_{60}$  molecules were converted to quantum dots, whereas the vibration modes of  $C_{60}$  referring to pentagon shear (Hg(7),  $\approx 1428 \text{ cm}^{-1}$ ), pentagon pinch (Ag(2),  $\approx 1469 \text{ cm}^{-1}$ ), and hexagon shear (Hg(8),  $\approx 1570 \text{ cm}^{-1}$ ) remained.<sup>[37,38]</sup> A new

band at  $\approx 1360 \text{ cm}^{-1}$  appeared in the spectrum of GOLQDs, corresponding to the D band representing defects.<sup>[39,40]</sup> The changes observed from Raman clearly demonstrate that the cage of  $C_{60}$  molecules has been broken into fragments by the modified Hummers processing, and pentagon and hexagon rings remain in the fragments.<sup>[41]</sup> X-ray diffraction of the GOLQD powder shown in Figure S3 (Supporting Information) also suggests that the characteristic peaks of bulk  $C_{60}$  disappeared.

Aggregated GOLQDs can self-assemble to form quasi-2D sheets, as demonstrated in the SEM image in Figure 1c and the TEM image in Figure S4a (Supporting Information) which was produced by dropping GOLQDs on an amorphous carbon film with micropores on Cu grids. Partially crystallized areas in the assembled GOLQDs were observed in a high resolution TEM (HRTEM) image (Figure S4b, Supporting Information). But the corresponding Fast Fourier Transformation (FFT) of the HRTEM image (inset of Figure S4b, Supporting Information) indicates d-spacings of 4.44 and 2.85 Å, which are larger than those of graphene. Figure 3c shows HRTEM images of individual GOLQDs on an amorphous carbon film obtained using a JEM-ARM200F instrument with a STEM  $C_s$  corrector at an acceleration voltage of 80 kV. One can clearly see the lattice marked by arrows in Figure 3c. Because of the existence of other carbon rings, e.g., pentagons induced by  $C_{60}$ , the lattice of GOLQDs differs from that of GQDs. The (100) lattice spacing of graphene or

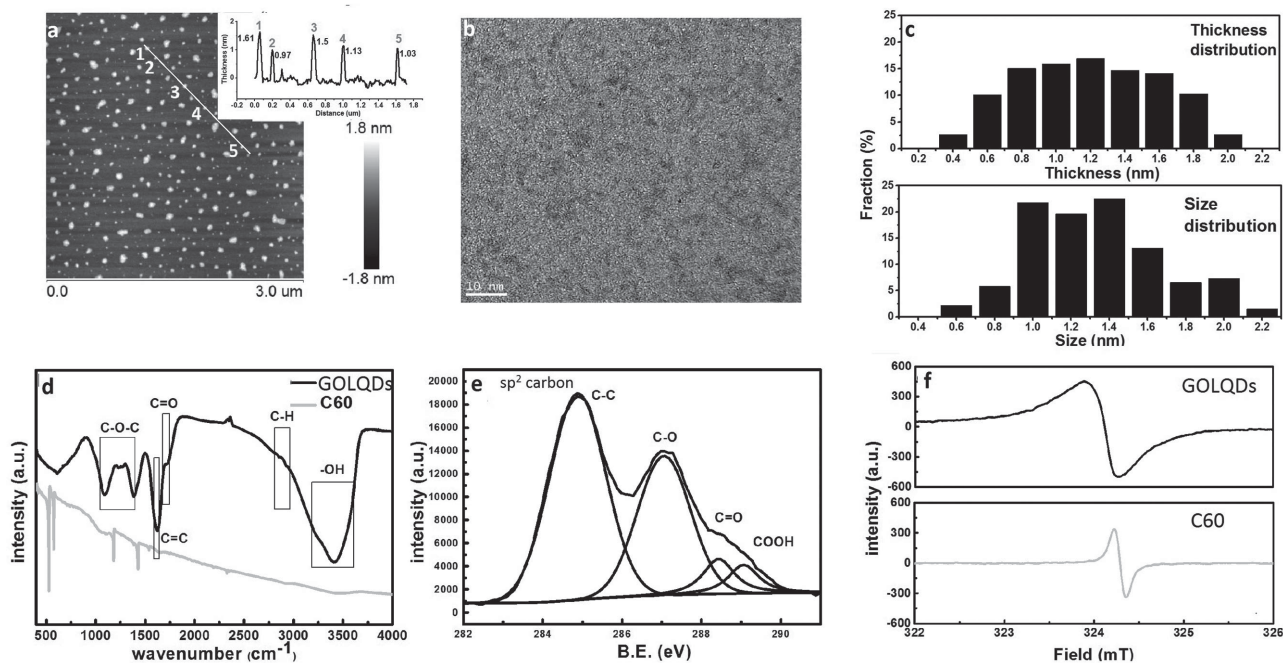


**Figure 2.** a) AFM topography image of GOLQDs. The heights of GOLQDs denoted by 1, 2, 3, 4, and 5 are shown in the inset with units of nm. b) TEM of isolated GOLQDs. c) Thickness distribution diagram (upper) and lateral size distribution diagram (lower) for GOLQDs. d) FT-IR and e) XPS C 1s spectra of GOLQD powder. f) EPR of GOLQD powder and C<sub>60</sub> powder.

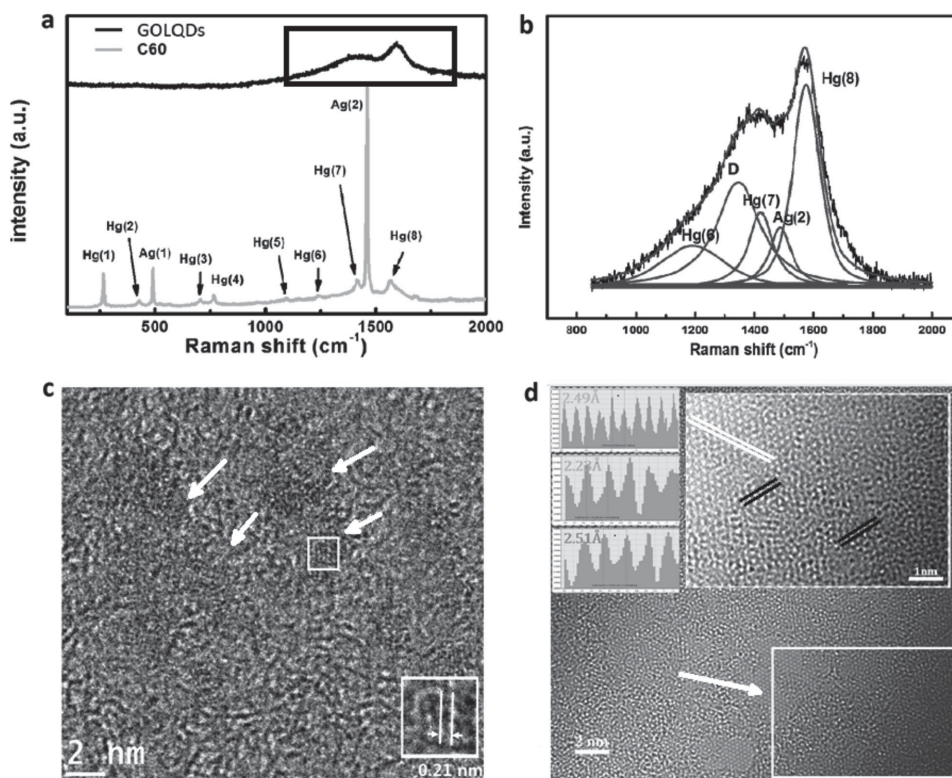


**Figure 3.** a) Raman spectra of GOLQDs and C<sub>60</sub>. b) Zoomed in the box in (a). c) HRTEM of individual GOLQDs on an amorphous carbon film on a Cu grid. The inset highlights the lattice of an area where hexagons dominate. d) HRTEM of aggregated GOLQDs on a graphene film on a Au grid, with arrows pointing to the graphene substrate. Inset shows an enlarged area, with the lattice constant of the graphene substrate (upper inset, white lines), and those of aggregated GOLQDs (middle and lower insets, dark lines).

GQDs, which is approximately 0.21 nm,<sup>[42]</sup> can be detected only in areas where hexagons dominate (inset of Figure 3c). To compare GOLQDs with graphene more directly, TEM specimens were also prepared by casting GOLQDs on graphene films on Au grids and characterized by aberration corrected TEM (Titan G2 cube 60-300) under an acceleration voltage of 80 kV as shown in Figure 3d. The typical lattice constant of aggregated GOLQDs varied between 2.23 and 2.51 Å, which is different from the measured lattice constant of graphene (2.49 Å) because of the existence of carbon rings other than hexagons.

## 2.2. Simulations and Structures

Oxidation of graphite with the modified Hummers method has been considered to be related to the intercalation and diffusion of the oxidizing agent, followed by subsequent hydrolysis.<sup>[43]</sup> With totally different structures, however, C<sub>60</sub> molecules (or assembled crystals of C<sub>60</sub>) should have different reaction pathways even in the same chemical environment. To aid in decoding the possible rupturing mechanism, we investigated the adsorption behavior of oxygen atoms on a C<sub>60</sub> molecule with first-principles calculations. Calculations were performed using a DFT method with the Perdew–Burke–Ernzerhof functional.<sup>[44]</sup> Calculation details can be found in the Supporting Information. As shown in Figure 4b, the first O atom prefers to adsorb on the C–C bond between hexagonal and pentagonal rings. After the first O atom is attached various adsorption sites were considered for an additional reaction with O, to find the energy favor site for O

adsorption and it was found that a second O atom attaches to the next neighboring C–C bond in the same hexagonal ring. As the number of O atom increases, as shown in Figure 4a–r, a possible path for the adsorption is to form a circle around the C<sub>60</sub> molecule. The average adsorption energy  $E_{\text{ads}}$  is defined as

$$E_{\text{ads}} = (E_{\text{oxidized C}_{60}} - E_{\text{C}_{60}} - m/2 \times E_{\text{O}_2}) / m \quad (1)$$

$E$  is the total energy of system denoted by subscript labels, and  $m$  is the number of attached oxygen atoms. Figure 5a shows the average adsorption energy per O atom on the C<sub>60</sub> molecule. Evidently, the oxidation of the C<sub>60</sub> molecule is exothermic. The values of average adsorption energy for the first three oxygen atoms decrease sharply. Then, for the 4th and further attached O atoms, the average adsorption energy oscillates with the increasing numbers of oxygen atoms, and varies between –1.6 and –1.7 eV. The adsorption of oxygen atoms on the C<sub>60</sub> molecule may induce the rupture of a C–C bond,<sup>[45,46]</sup> which enables it to be cut into pieces.

The electronic structure of as-prepared GOLQDs was investigated with UV–vis–NIR absorption spectroscopy carried out on the GOLQD suspension (0.112 mg mL<sup>–1</sup>) and a GOLQD film made by casting and drying droplets of the GOLQD suspension on a quartz substrate. The spectrum from the suspension shown in Figure 5b indicates two peaks, namely, bond A (≈215 nm) and bond B (≈260 nm), which are respectively due to the  $\pi$ – $\pi^*$  transition of aromatic C=C bonds and n– $\pi^*$  transition of C=O bonds.<sup>[47]</sup> The  $\pi$ – $\pi^*$  transition peak of aromatic C=C bonds was also observed

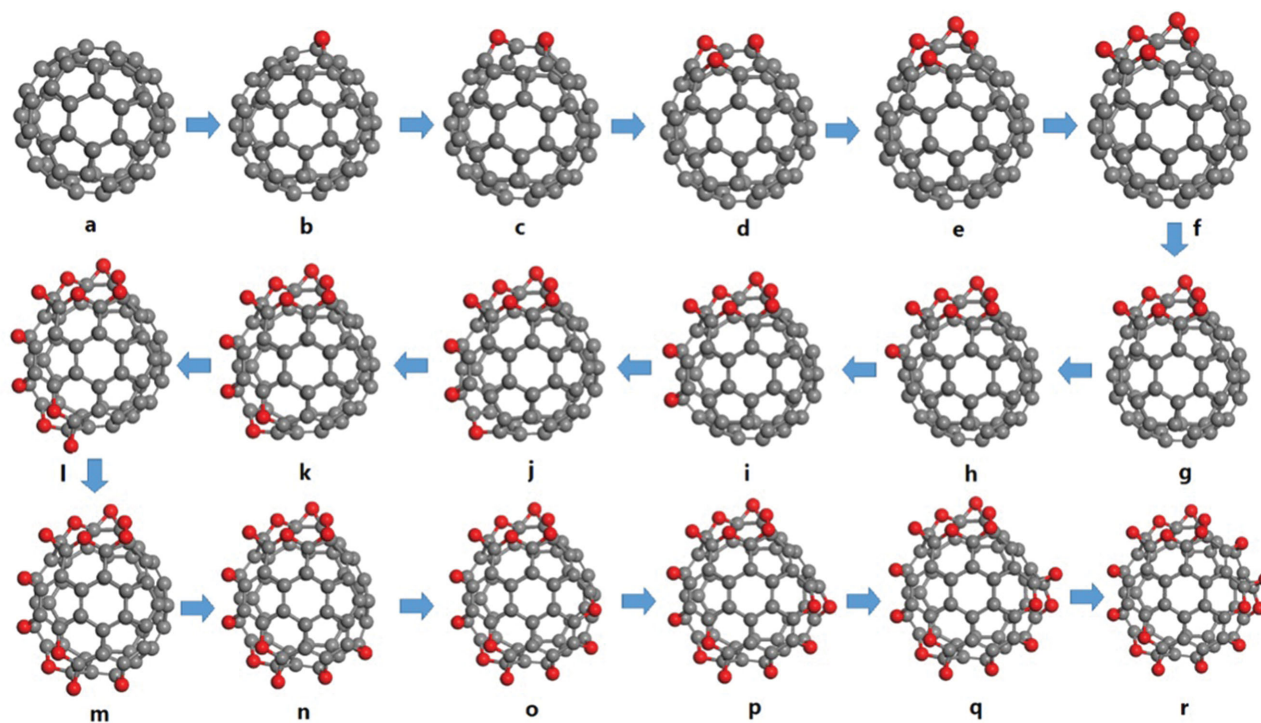
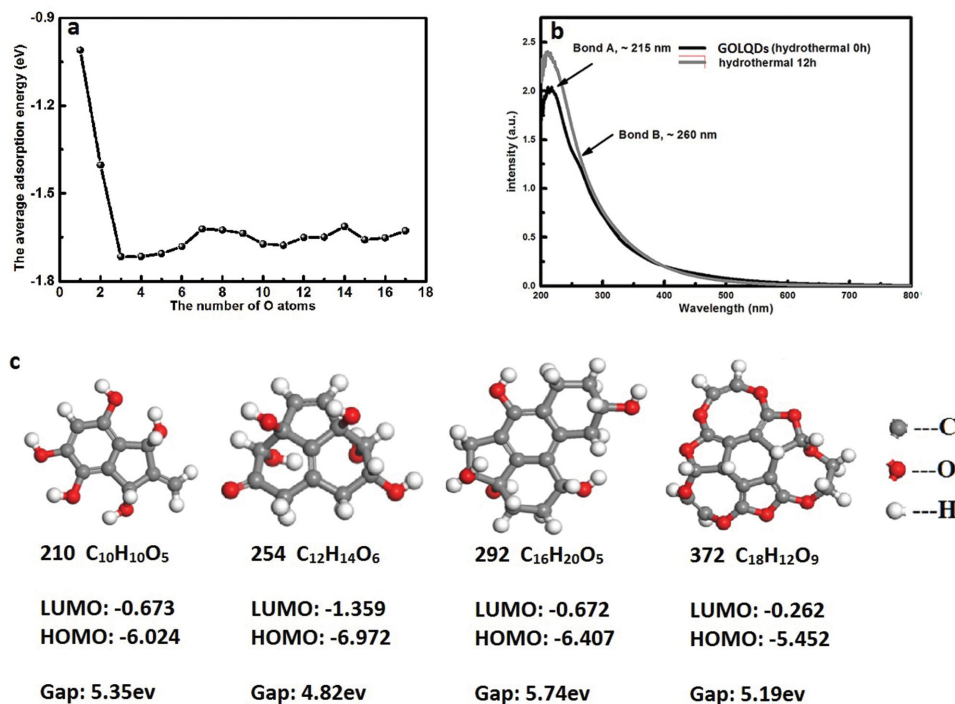


Figure 4. Simulated adsorption sequence of oxygen atoms on a C<sub>60</sub> molecule.



**Figure 5.** a) Average adsorption energy calculated by the formula:  $E_{\text{ads}} = (E_{\text{oxidized C}_{60}} - E_{\text{C}_{60}} - m/2 \times E_{\text{O}_2})/m$ , where  $E$  is the total energy of system denoted by subscript labels, and  $m$  is the number of attached oxygen atoms. b) UV-vis-NIR absorption spectra. Bond A ( $\approx 215$  nm) and bond B ( $\approx 260$  nm) represent the  $\pi$ - $\pi^*$  transition of aromatic C=C bonds and  $n$ - $\pi^*$  transition of C=O bonds, respectively. c) Possible molecular structures and their energy gaps calculated by DFT-B3LYP.

from the dried GOLQDs film, although the value shifted to  $\approx 250$  nm (Figure S5, Supporting Information). Such a bathochromic shift may be caused by the change in electronic conjugation,<sup>[48,49]</sup> which is possibly induced by changes in the morphology of GOLQDs produced during drying. Matrix-assisted laser desorption/ionization time-of-flight mass spectrometry (MALDI-TOF-MS) was used to explore possible molecular weights of the as-prepared GOLQD in suspension (Figure S6, Supporting Information). As can be seen from the spectrum, various molecules with mass lower than 720 amu (the molecular weight of C<sub>60</sub>) were found in the suspension. Based on the energy gap determined by UV-vis-NIR spectroscopy and molecular weights obtained from MALDI-TOF-MS, we attempted to construct the possible structure of the GOLQDs. However, given the multiple possibilities regarding the topological features of oxygen-containing groups (hydroxyl, carbonyl, epoxy, and carboxyl) on GOLQDs, matching molecular structures with all the mass peaks from the MALDI-TOF-MS spectra is impossible. A few possible structures corresponding to the mass peaks of 210, 254, 292, and 372 amu are shown in Figure 5c in which, for simplification, we have considered only pentagons, hexagons, and possible oxygen-containing groups in the structures. To evaluate the energy gap between the highest occupied molecule orbital (HOMO) and the lowest unoccupied molecule orbital (LUMO) of GOLQDs, a hybrid DFT method (B3LYP) was used.<sup>[50-53]</sup> Energy convergence was set to  $10^{-5}$  Ha, and force convergence was set to  $10^{-3}$  Ha  $\text{\AA}^{-1}$  for geometry optimization. For electronic structure calculation, the energy convergence was increased to  $10^{-6}$  Ha. The calculated energy

positions of HOMO and LUMO, as well as their energy gaps, are listed in Figure 5c. The calculated energy gap for each is  $\approx 5$  eV, which is consistent with the experimental spectra.

### 2.3. Photoluminescence

Light from a xenon lamp with wavelengths between 320 and 520 nm was used to excite PL from a GOLQD suspension with a concentration of  $\approx 0.17$  mg mL<sup>-1</sup> (Figure 6a). As seen from the spectra, GOLQDs emit luminescence through a down conversion process. The intensity and position of PL peaks excited by different wavelengths are shown in the inset of Figure 6a. The PL peak red-shifts from 450 to 570 nm as the excitation wavelength increases from 320 to 520 nm. PL intensity increases when the excitation wavelength is increased from 320 to 360 nm, then decreases for longer excitation wavelengths. The broad PL peaks are attributed to the broad size distribution of GOLQDs in the suspension. The band gaps of GOLQDs are known to depend on size when the size is lower than their Bohr radius.<sup>[54,55]</sup> As an upper limit, one benzene ring possesses a band gap of  $\approx 7$  eV, and the band gap becomes smaller as the number of hexagonal rings increases.<sup>[56]</sup> Our simulations have also shown that the addition of pentagons to hexagons lowers the band gap (Figure S7, Supporting Information), explaining the experimental observation of excitation and luminescence in the visible range. When being excited with a 325 nm laser, the PL of GOLQDs also can be observed from a solid polyethylene glycol-800 (PEG<sub>800N</sub>) solid film made by dispersing GOLQDs

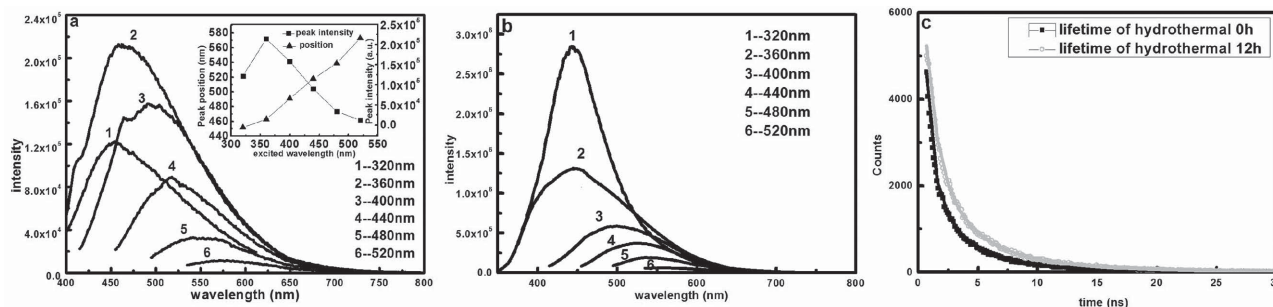


**Figure 6.** a) PL spectra of GOLQDs in suspension. Excited wavelength changes from 320 to 500 nm with an interval of 40 nm. The inset figure shows the dependence of emission peak position and intensity on the excitation wavelength. b) PL spectra of GOLQDs hydrothermally treated at 160 °C for 12 h. c) Lifetime measurement before and after hydrothermal treatment. Excitation and emission wavelengths are 420 and 520 nm, respectively. Function  $I(t) = A_1e^{-x/t_1} + A_2e^{-x/t_2} + A_3e^{-x/t_3}$  was used for fitting. The average lifetime was calculated by  $t_{\text{average}} = (A_1t_1 + A_2t_2 + A_3t_3)/(A_1 + A_2 + A_3)$ .

in PEG<sub>800N</sub> followed by drying, as shown by Figure S8 (Supporting Information).

To investigate the effects of oxygen-containing groups on PL, a hydrothermal treatment at 160 °C for 12 h was performed on the GOLQD suspension to partially remove oxygen-containing groups. Raman spectra (Figure S9, Supporting Information) show that  $I_D/I_G$  changes from 0.87 to 0.80 after this hydrothermal treatment, whereas XPS spectra (Figure S9, Supporting Information) show C/O atomic ratio changes from 1.12 to 1.64. In addition, the UV-vis-NIR absorption spectrum (Figure 5b) shows that the band representing  $n-\pi^*$  transition of C=O bonds disappears. These results all clearly indicate the decrease in the number of oxygen-containing groups after hydrothermal treatment. The PL spectra of the hydrothermally treated samples shown in Figure 6b indicate that the maximum intensity of PL emission occurs at an excitation wavelength of 320 nm instead of 360 nm, in contrast to the samples before the treatment. At the same time, PL intensity significantly increases after hydrothermal treatment for 12 h (Figure S10, Supporting Information), leading to a ten-fold increase in quantum yield (QY), from 0.28% to 2.7% (Table S2, Supporting Information). This result suggests that oxygen-containing groups may act as quenching sites for the PL of as-prepared GOLQDs. A previous study showed that carboxylic and epoxide groups could act as nonradiative electron-hole recombination centers, and that the removal of these groups improved quantum yield.<sup>[57]</sup>

Transient fluorescence spectra were obtained to investigate GOLQD PL lifetime. Figure 6c compares the PL decay for samples before and after hydrothermal treatment. Fitting the decay curves to three exponential functions suggests that the average lifetime for each curve contains one fast and two slow components, which are considered to be caused by the fast band-gap transition and those related to oxygen-related transition, respectively.<sup>[58–61]</sup> One can clearly see that hydrothermal treatment has increased the average lifetime from 2.01 to 2.67 ns, which indicates that the recombination pathway of electron-hole pairs was changed after the oxygen-containing groups were partially removed. More hydrothermal treatments (Figure S10, Supporting Information) and the corresponding lifetime measurements

after each treatment (Figure S11 and Table S1, Supporting Information) suggest that the lifetime and the proportion of the fast band-gap transition in total PL increase as the duration of the hydrothermal treatment increases. With the removal of oxygen-containing groups, the number of nonradiative traps decreases. The decrease in the number of nonradiative traps leads to an increase of fast band-gap transition that increases the entire PL lifetime.

## 2.4. Catalytic Application

Because of its many oxygen functional groups, graphene oxide has been investigated to catalyze the oxidation of alcohols.<sup>[62,63]</sup> GOLQDs have more edges and higher ratios of oxygen groups and thus may be able to demonstrate higher catalytic activity. To measure the catalytic performance, GOLQDs were dispersed in benzyl alcohol (the GOLQDs loading was 0.2 wt%) and the mixture was stirred for 6 d at 100 °C with reflux under an air atmosphere. Comparing the 400 MHz <sup>1</sup>H NMR spectra of the dispersion in **Figure 7**, the dispersion resulting from a 6 d reaction shows signs of benzaldehyde. To determine whether ambient oxygen was the oxidant, the reaction was also performed under a nitrogen atmosphere with other conditions remaining the same, and <sup>1</sup>H NMR spectra of the resulting dispersion shows no benzaldehyde signal (see Figure S12, Supporting Information). The conversion was estimated by integration of the aldehyde peak (around 10 ppm) of benzaldehyde versus the hydroxyl peak (around 3.7 ppm) of benzyl alcohol. As shown in Figure 7, the weight percentage of benzaldehyde in the resulting dispersion was 4.8% and the turnover number, calculated as the ratio of benzaldehyde mol to GOLQDs mass, is 0.226, which is much higher than 0.018 (5 wt% GO loading), 0.012 (20 wt% GO loading), and 0.013 (50 wt% GO loading) in a previous report.<sup>[62]</sup>

## 3. Conclusions

We achieved the large-scale synthesis of GOLQDs by “chemically rupturing” C<sub>60</sub> molecules using a modified Hummers

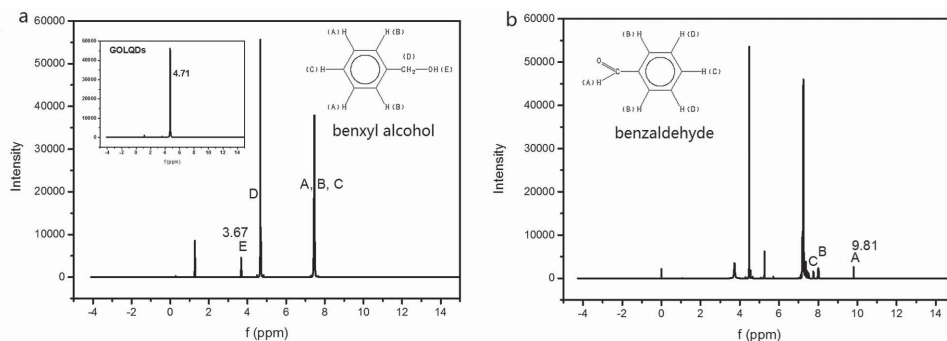


**Figure 7.** a)  $^1\text{H}$  NMR of benzyl alcohol ( $\text{CDCl}_3$  as buffering). Hydroxyl H peak (E position of benzyl alcohol) is at 3.67 ppm. Inset:  $^1\text{H}$  NMR of GOLQDs suspension ( $\text{D}_2\text{O}$  as buffering). b)  $^1\text{H}$  NMR of mixture of GOLQDs and benzyl alcohol reacting at  $100^\circ\text{C}$  for 6 d ( $\text{CDCl}_3$  as buffering). The integrated peak areas at 9.81 ppm (representing aldehyde H, A position of benzaldehyde) versus at 3.67 ppm (representing hydroxy H, E position of benzyl alcohol) are 0.05 and 1, respectively. The sum of benzaldehyde and benzyl alcohol is 100%; the weight percentage of benzaldehyde is 4.8%.

method. The production yield of  $\sim 25$  wt% is higher than previously reported yields of other quantum dots based on  $sp^2$  carbon. With pentagons in the structure, the curved GOLQDs have uniform height and size distributions. Our DFT study indicates that oxidation may start from the insertion of oxygen atoms in C–C bonds, and that the band gap of GOLQDs is lowered by the presence of pentagons in the carbon framework. The PL of as-prepared GOLQDs may be attributed to effects of size confinement and oxygen-containing groups. Defect states related to oxygen-containing groups seem to form emissive traps that induce nonradiative emission, which is supported by the order of magnitude higher quantum yield and longer excitation lifetime, when oxygen-containing groups are partially removed. In addition, we demonstrated that GOLQDs are a highly efficient oxidization catalyst, which shows an order of magnitude higher conversion efficiency than graphene oxide when used to oxidize benzyl alcohol to benzaldehyde.

## Supporting Information

Supporting Information is available from the Wiley Online Library or from the author.

## Acknowledgements

Y. Zhu appreciates support from China Government 1000 plan Talent Program, China MOE NCET program, Natural Science Foundation of China (51322204), and the Fundamental Research Funds for the Central Universities (WK2060140014). X. Wu is supported by NKBRPC (Grant Nos. 2011CB921400 and 2012CB922001), NSFC (Grant Nos. 51172223 and 21121003), Strategic Priority Research Program of CAS (XDB01020300), and the National Program for Support of Top-notch Young Professionals. N. Y. Kim, Z. Lee, and R. S. Ruoff appreciate support from the Institute of Basic Science, Korea. All authors appreciate the helpful editing from Dr. Peter Thrower.

- [1] K. S. Novoselov, A. K. Geim, S. V. Morozov, D. Jiang, Y. Zhang, S. V. Dubonos, I. V. Grigorieva, A. A. Firsov, *Science* **2004**, *306*, 666.
- [2] A. K. Geim, K. S. Novoselov, *Nat. Mater.* **2007**, *6*, 183.
- [3] K. S. Novoselov, D. Jiang, F. Schedin, T. J. Booth, V. V. Khotkevich, S. V. Morozov, A. K. Geim, *Proc. Natl. Acad. Sci. USA* **2005**, *102*, 10451.
- [4] L. A. Ponomarenko, F. Schedin, M. I. Katsnelson, R. Yang, E. W. Hill, K. S. Novoselov, A. K. Geim, *Science* **2008**, *320*, 356.
- [5] S. J. Zhu, J. H. Zhang, C. Y. Qiao, S. J. Tang, Y. F. Li, W. J. Yuan, B. Li, L. Tian, F. Liu, R. Hu, H. N. Gao, H. T. Wei, H. Zhang, H. C. Sun, B. Yang, *Chem. Commun.* **2011**, *47*, 6858.
- [6] K. Nakada, M. Fujita, G. Dresselhaus, M. S. Dresselhaus, *Phys. Rev. B* **1996**, *54*, 17954.
- [7] H. T. Li, X. D. He, Z. H. Kang, H. Huang, Y. Liu, J. L. Liu, S. Y. Lian, C. H. A. Tsang, X. B. Yang, S. T. Lee, *Angew. Chem. Int. Ed.* **2010**, *49*, 4430.
- [8] X. Yan, B. S. Li, X. Cui, Q. S. Wei, K. Tajima, L. S. Li, *J. Phys. Chem. Lett.* **2011**, *2*, 1119.
- [9] M. Y. Han, B. Ozyilmaz, Y. B. Zhang, P. Kim, *Phys. Rev. Lett.* **2007**, *98*, 206805.
- [10] Y. W. Son, M. L. Cohen, S. G. Louie, *Phys. Rev. Lett.* **2006**, *97*, 216803.
- [11] X. L. Li, X. R. Wang, L. Zhang, S. W. Lee, H. J. Dai, *Science* **2008**, *319*, 1229.
- [12] M. Koch, F. Ample, C. Joachim, L. Grill, *Nat. Nanotechnol.* **2012**, *7*, 713.
- [13] R. T. Weitz, U. Zschieschang, F. Effenberger, H. Klauk, M. Burghard, K. Kern, *Nano. Lett.* **2007**, *7*, 22.
- [14] J. Peng, W. Gao, B. K. Gupta, Z. Liu, R. Romero-Aburto, L. H. Ge, L. Song, L. B. Alemany, X. B. Zhan, G. H. Gao, S. A. Vithayathil, B. A. Kaiparettu, A. A. Marti, T. Hayashi, J. J. Zhu, P. M. Ajayan, *Nano. Lett.* **2012**, *12*, 844.
- [15] D. Y. Pan, J. C. Zhang, Z. Li, M. H. Wu, *Adv. Mater.* **2010**, *22*, 734.
- [16] J. H. Shen, Y. H. Zhu, C. Chen, X. L. Yang, C. Z. Li, *Chem. Commun.* **2011**, *47*, 2580.
- [17] Z. A. Qiao, Y. F. Wang, Y. Gao, H. W. Li, T. Y. Dai, Y. L. Liu, Q. S. Huo, *Chem. Commun.* **2010**, *46*, 8812.
- [18] X. Yan, X. Cui, B. S. Li, L. S. Li, *Nano Lett.* **2010**, *10*, 1869.
- [19] X. Yan, X. Cui, L. S. Li, *J. Am. Chem. Soc.* **2010**, *132*, 5944.
- [20] L. B. Tang, R. B. Ji, X. K. Cao, J. Y. Lin, H. X. Jiang, X. M. Li, K. S. Teng, C. M. Luk, S. J. Zeng, J. H. Hao, S. P. Lau, *ACS Nano* **2012**, *6*, 5102.
- [21] Y. Q. Dong, J. W. Shao, C. Q. Chen, H. Li, R. X. Wang, Y. W. Chi, X. M. Lin, G. N. Chen, *Carbon* **2012**, *50*, 4738.
- [22] Y. Li, Y. Hu, Y. Zhao, G. Q. Shi, L. E. Deng, Y. B. Hou, L. T. Qu, *Adv. Mater.* **2011**, *23*, 776.

- [23] D. B. Shinde, V. K. Pillai, *Chem.-Eur. J.* **2012**, *18*, 12522.
- [24] L. X. Lin, S. W. Zhang, *Chem. Commun.* **2012**, *48*, 10177.
- [25] R. Q. Ye, C. S. Xiang, J. Lin, Z. W. Peng, K. W. Huang, Z. Yan, N. P. Cook, E. L. G. Samuel, C. C. Hwang, G. D. Ruan, G. Ceriotti, A. R. O. Raji, A. A. Marti, J. M. Tour, *Nat. Commun.* **2013**, *4*, 2943.
- [26] L. L. Li, G. H. Wu, G. H. Yang, J. Peng, J. W. Zhao, J. J. Zhu, *Nanoscale* **2013**, *5*, 4015.
- [27] J. Lu, P. S. E. Yeo, C. K. Gan, P. Wu, K. P. Loh, *Nat. Nanotechnol.* **2011**, *6*, 247.
- [28] C. K. Chua, Z. Sofer, P. Simek, O. Jankovsky, K. Klimova, S. Bakardjieva, S. H. Kuckova, M. Pumera, *ACS Nano* **2015**, *9*, 2548.
- [29] W. S. Hummers, R. E. Offeman, *J. Am. Chem. Soc.* **1958**, *80*, 1339.
- [30] Y. W. Zhu, S. Murali, W. W. Cai, X. S. Li, J. W. Suk, J. R. Potts, R. S. Ruoff, *Adv. Mater.* **2010**, *22*, 5226.
- [31] X. B. Fan, W. C. Peng, Y. Li, X. Y. Li, S. L. Wang, G. L. Zhang, F. B. Zhang, *Adv. Mater.* **2008**, *20*, 4490.
- [32] S. Park, J. An, J. R. Potts, A. Velamakanni, S. Murali, R. S. Ruoff, *Carbon* **2011**, *49*, 3019.
- [33] S. Stankovich, R. D. Piner, X. Q. Chen, N. Q. Wu, S. T. Nguyen, R. S. Ruoff, *J. Mater. Chem.* **2006**, *16*, 155.
- [34] C. Gomez-Navarro, R. T. Weitz, A. M. Bittner, M. Scolari, A. Mews, M. Burghard, K. Kern, *Nano Lett.* **2007**, *7*, 3499.
- [35] S. H. Jin, D. H. Kim, G. H. Jun, S. H. Hong, S. Jeon, *ACS Nano* **2013**, *7*, 1239.
- [36] F. Liu, M. Jang, H. D. Ha, J. Kim, Y. Cho, T. S. Seo, *Adv. Mater.* **2013**, *25*, 3657.
- [37] Y. Iwasa, T. Arima, R. M. Fleming, T. Siegrist, O. Zhou, R. C. Haddon, L. J. Rothberg, K. B. Lyons, H. L. Carter, A. F. Hebard, R. Tycko, G. Dabbagh, J. J. Krajewski, G. A. Thomas, T. Yagi, *Science* **1994**, *264*, 1570.
- [38] C. S. Yoo, W. J. Nellis, *Science* **1991**, *254*, 1489.
- [39] A. C. Ferrari, J. C. Meyer, V. Scardaci, C. Casiraghi, M. Lazzeri, F. Mauri, S. Piscanec, D. Jiang, K. S. Novoselov, S. Roth, A. K. Geim, *Phys. Rev. Lett.* **2006**, *97*, 187401.
- [40] A. C. Ferrari, *Solid State Commun.* **2007**, *143*, 47.
- [41] L. Wang, B. B. Liu, H. Li, W. G. Yang, Y. Ding, S. V. Sinogeikin, Y. Meng, Z. X. Liu, X. C. Zeng, W. L. Mao, *Science* **2012**, *337*, 825.
- [42] W. Kwon, Y. Kim, C. Lee, M. Lee, H. C. Choi, T. Lee, S. Rhee, *Nano Lett.* **2014**, *14*, 1306.
- [43] A. M. Dimiev, J. M. Tour, *ACS Nano* **2014**, *8*, 3060.
- [44] J. P. Perdew, K. Burke, M. Ernzerhof, *Phys. Rev. Lett.* **1996**, *77*, 3865.
- [45] J. L. Li, K. N. Kudin, M. J. McAllister, R. K. Prud'homme, I. A. Aksay, R. Car, *Phys. Rev. Lett.* **2006**, *96*, 176101.
- [46] P. M. Ajayan, B. I. Yakobson, *Nature* **2006**, *441*, 818.
- [47] L. Lin, S. Zhang, *Chem. Commun.* **2012**, *48*, 10177.
- [48] J. I. Paredes, S. Villar-Rodil, A. Martinez-Alonso, J. M. D. Tascon, *Langmuir* **2008**, *24*, 10560.
- [49] D. Li, M. B. Muller, S. Gilje, R. B. Kaner, G. G. Wallace, *Nat. Nanotech.* **2008**, *3*, 101.
- [50] A. D. Becke, *J. Chem. Phys.* **1993**, *98*, 5648.
- [51] C. T. Lee, W. T. Yang, R. G. Parr, *Phys. Rev. B* **1988**, *37*, 785.
- [52] S. H. Vosko, L. Wilk, M. Nusair, *Can. J. Phys.* **1980**, *58*, 1200.
- [53] P. J. Stephens, F. J. Devlin, C. F. Chabalowski, M. J. Frisch, *J. Phys. Chem.-Us* **1994**, *98*, 11623.
- [54] X. Michalet, F. F. Pinaud, L. A. Bentolila, J. M. Tsay, S. Doose, J. J. Li, G. Sundaresan, A. M. Wu, S. S. Gambhir, S. Weiss, *Science* **2005**, *307*, 538.
- [55] W. C. W. Chan, S. M. Nie, *Science* **1998**, *281*, 2016.
- [56] G. Eda, Y. Y. Lin, C. Mattevi, H. Yamaguchi, H. A. Chen, I. S. Chen, C. W. Chen, M. Chhowalla, *Adv. Mater.* **2010**, *22*, 505.
- [57] K. P. Loh, Q. L. Bao, G. Eda, M. Chhowalla, *Nat. Chem.* **2010**, *2*, 1015.
- [58] D. S. English, L. E. Pell, Z. H. Yu, P. F. Barbara, B. A. Korgel, *Nano Lett.* **2002**, *2*, 681.
- [59] L. Bao, Z. L. Zhang, Z. Q. Tian, L. Zhang, C. Liu, Y. Lin, B. P. Qi, D. W. Pang, *Adv. Mater.* **2011**, *23*, 5801.
- [60] X. Wang, L. Cao, S. T. Yang, F. S. Lu, M. J. Mezziani, L. L. Tian, K. W. Sun, M. A. Bloodgood, Y. P. Sun, *Angew. Chem. Int. Ed.* **2010**, *49*, 5310.
- [61] S. Sato, M. T. Swihart, *Chem. Mater.* **2006**, *18*, 4083.
- [62] D. R. Dreyer, H. P. Jia, C. W. Bielawski, *Angew. Chem. Int. Ed.* **2010**, *49*, 6813.
- [63] D. R. Dreyer, S. Murali, Y. Zhu, R. S. Ruoff, C. W. Bielawski, *J. Mater. Chem.* **2011**, *21*, 3443.

Received: June 7, 2015  
 Revised: July 4, 2015  
 Published online: August 19, 2015